Mitigation of Environmental Temperature Variation Effects in OCDMA Networks Using PSO Power Control

Alysson José dos Santos, Fábio Renan Durand, and Taufik Abrão

***Abstract*—In this paper, a mitigation of environmental temperature variation effects in optical code division multiple access (OCDMA) networks based on power control is described. The temperature changes would adversely affect 2D wavelength-hopping time-spreading optical code by causing a reduction in the expected height of the autocorrelation peak. Environmental temperature variation is usually difficult to accurately determine and compensate for due to its dynamic nature and fluctuations. Furthermore, the power control strategy allows the regulation of the transmitted power in order to dynamically mitigate the effects of temperature variation. The particle swarm optimization (PSO) algorithm is evocated to solve the problem of power control based on the signal-to-noise plus interference ratio optimization to mitigate the environmental effects. Afterward, numerical results are discussed taking into account the code parameters, such as the code weight and spectral spacing.**

***Index Terms*—Heuristic search; Optical networks; Particle swarm optimization; Power control; Signal-to-noise plus interference ratio.**

I. Introduction

The diversity and volume of the traffic transmitted in all the scales of the networks results in the high effort to improve the technology of transmission, switching, control, and management of optical networks [1,2]. In this context, the increase of the heterogeneous set of requirements caused by massive intensification of content-delivery networks and data centers is spurring rapid growth in metro-only Internet traffic [1]. Moreover, the advances of technologies such as optical code division multiple access (OCDMA), orthogonal frequency division multiplexing (OFDM), and wavelength division multiplexing (WDM) are strategic to support the traffic requirements [1–3]. Over the last few years, OCDMA-based networks have attracted a lot of interest due to their various advantages including asynchronous operation, high network flexibility, protocol transparency, simplified network control, and potentially enhanced security [3,4]. Moreover, this technology can meet a broad range of services with different and variable demands of bit rate, connection duration, frequency of use, and setup time [4]. Hence, OCDMA networks can be controlled at the physical layer to adapt to traffic variations and customer demands [5]. In OCDMA networks, each different code defines a user and different code-users can share a common channel. In a common channel, the interference that may arise between different code-users is known as multiple access interference (MAI) and can limit the number of code-users utilizing the channel simultaneously [3]. Furthermore, the establishment of transmissions with a higher optical signal-to-noise plus interference ratio (SNIR) allows us to reduce the number of retransmissions by higher layers, thus increasing network throughput [6].

The physical impairments composed by linear and nonlinear effects degrade the signal quality of transmission (QoT) and significantly affect the overall performance of optical communication systems. Linear effects such as group velocity dispersion (GVD), polarization mode dispersion (PMD), and amplified spontaneous emission (ASE) are independent of the power level in the fiber [7]. On other hand, the main nonlinear impairments, which depend on the power level, include self-phase modulation (SPM), cross-phase modulation (XPM), and four-wave mixing (FWM) [7]. These linear and nonlinear impairments depend on various factors such as the power level, distance of links, and bit rate, as well the optical code parameters' characteristics [6–9]. Besides, these effects have been extensively studied, and various mitigation techniques have been proposed [6–9].

In this context, environmental temperature variation became an important issue in the signal QoT degradation in OCDMA networks based on 2D codes (time/wavelength) [10]. The environmental temperature variation is usually difficult to accurately determine and compensate for due to its dynamic nature and fluctuations [11]. In these cases, besides pulse broadening and peak power reduction, the effects of environmental temperature variation include time skewing. Time skewing is the phenomenon in which temporal spreading of multiwavelength pulses and relative delays occur among chips at different wavelengths [12]. Furthermore, pulse broadening, peak power reduction,

Manuscript received February 5, 2015; revised May 1, 2015; accepted June 18, 2015; published July 8, 2015 (Doc. ID 233601).

A. J. dos Santosis with the WEG Electrical Motors, Jaraguá do Sul-SC, Brazil.

F. R. Durand (e-mail: fabiodurand@utfpr.edu.br) is with the Universidade Tecnológica Federal do Paraná, UTFPR, Cornélio Procópio-PR, Brazil.

T. Abrão is with the Department of Electrical Engineering, State University of Londrina, UEL-PR, Londrina, Brazil.

http://dx.doi.org/10.1364/JOCN.7.000707

and time skewing caused by environmental temperature variation results in incorrect decoding and then errors in bit detection. Moreover, even for links with full compensation for dispersion the effects from environmental temperature variation cannot be neglected [10].

The mitigation of the environmental temperature variation effects on 2D OCDMA networks encompasses the code parameter optimization, such as spectral spacing reduction [10], or an intelligent fuzzy system to adequate the better code weight [13]. In the former, the temporal skewing is controlled based on adjusting the code spectral allocation and the spectral spacing between the individual wavelengths used in the code formation. On the other hand, in the latter, an intelligent fuzzy system can *a priori* compensate for code weight at the encoder, according to estimations of environmental temperature variations provided by external sensor networks.

In this context, this paper proposes and analyzes for the first time, to the best of our knowledge, the power control of transmitted power, based on particle swarm optimization (PSO), in order to dynamically mitigate the effects of temperature variation with low cost and complexity. The intensity of the transmitted optical signal is directly adjusted from the laser source with respect to the target SNIR by the PSO algorithm. The optimization method based on the heuristic PSO approach is attractive due to its performance-complexity trade-off and fairness features, the optimization methods that deploy matrix inversion, purely numerical procedures, and other heuristic approaches [5,14]. Furthermore, for comparison purposes, we have included numerical results for the heuristic optimization technique based on ant colony optimization (ACO), aiming to validate and demonstrate the effectiveness of heuristic approaches over deterministic matrix inversion methods.

The paper is organized in the following manner: in Section II the OCDMA network based on 2D codes is described, while in Section III the environmental temperature variation effects are illustrated. In Section IV the power control strategy to mitigate the environmental temperature variation is discussed. Numerical results are presented in Section V. Finally, the main conclusions are offered in Section VI.

II. Network Architecture

A. OCDMA Network

The OCDMA network considered in this work is formed by $K \times K$ nodes interconnected by a passive star coupler, in a broadcast-and-select pattern as shown in Fig. 1. The transmitting and receiving nodes create a virtual path based on the code, and the total link length is given by

$$d_{ij} = d_i^{tx} + d_j^{rx}, \tag{1}$$

where d_i^{tx} is the link length from the transmitting node to the star coupler and d_j^{rx} is the link length from the receiving node to the star coupler. The received power at a jth node is given by

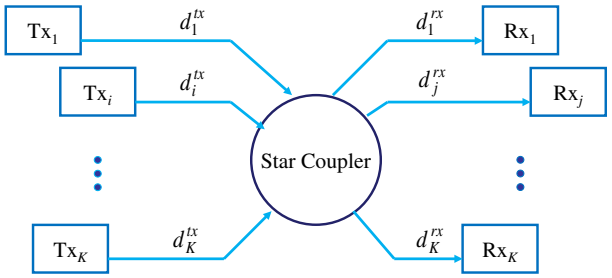

Fig. 1. OCDMA network architecture.

$$P_{rj} = a_{\text{star}} p_i \exp(-\alpha_f d_{ij}), \tag{2}$$

where p_i is the transmitted power by the ith transmitter node, α_f is the fiber attenuation (km^{-1}), and a_{star} is the star coupler attenuation (linear units). Considering decibel units [15],

$$a_{\text{satr}} = 10 \log(K) - [10 \log_2(K) \log_{10}(\delta)], \tag{3}$$

where δ is the excess loss ratio. For viability characteristics, we consider that network equipment, such as code-processing devices (encoders and decoders at the transmitter and receiver) and star couplers, could be made using robust, lightweight, and low-cost technology platforms with commercial-off-the-shelf technologies [16].

B. 2D OCDMA Codes

In the 2D wavelength-hopping/time-spreading code sequence OCDMA network the code is transmitted and its destiny in the network is determined by a particular code sequence [3]. The 2D codes can be represented by $N_\lambda \times N_T$ matrices, where N_λ is the number of rows, which is equal to the number of available wavelengths, and N_T is the number of columns, which is equal to the code length [3]. The code length is determined by the bit period T_B, which is subdivided into small units called chips, each of duration $T_c = T_B/N_T$. In each code, there are w short pulses of different wavelength, where w is called the weight of the code. An $(N_\lambda \times N_T, w, I_a, I_c)$ code is a collection of binary $N_\lambda \times N_T$ matrices each of code weight w; I_a and I_c are nonnegative integers and represent the constraints on the autocorrelation and cross correlation [4], respectively.

III. Effects of Environmental Temperature Variation

In 2D OCDMA codes, besides pulse broadening and peak power reduction, the effects of dispersion include time skewing [3]. This effect, associated with GVD and PMD, presents dynamic behavior and fluctuations induced by external stress/strain applied to the fiber after installation, as well as by changing environmental conditions [3,10]; however, dispersion effects such GVD and PMD can be effectively compensated for by a fully dispersion compensated

link [7,10]. On the other hand, the change in the environmental conditions, such as environmental temperature variation, is difficult to accurately determine and compensate due to its dynamic nature and fluctuations [11]. This effect occurs because the optical fibers could be exposed to temperature variations up to about 20 ± °C, since optical cables are buried at a depth of about 2–4 feet below the ground [11]. The fiber temperature changes would adversely affect 2D wavelength-hopping time-spreading optical code, thanks to the character of the fiber thermal coefficient, by the reduction in the expected height of the autocorrelation peak [10]. Moreover, the autocorrelation signal is distorted due to a temperature-induced temporal skewing effect. This induced skewing affects the code and the height, shape, and width of the decoded autocorrelation signal. Besides, the severity of this effect depends on the temperature change magnitude (ΔT) and the link length (d_{ij}).

The temperature variation induced temporal skew (Δt) is given by [10]

$$\Delta t = D_{\text{temp}} \times \Delta T \times \Delta\Lambda \times d_{ij}, \tag{4}$$

where D_{temp} (ps/nm·km/°C) is the thermal coefficient of the fiber, ΔT (°C) is the average change in temperature experienced by the buried fiber, $\Delta\Lambda$ (nm) is the spectral spacing between code wavelength pulses, and d_{ij} is the ijth link length.

The amount of pulsewidth shrinking ($\Delta\tau$) for each wavelength pulse is given by [10]

$$\Delta\tau = D_{\text{temp}} \times \Delta T \times \Delta\lambda \times d_{ij}, \tag{5}$$

where $\Delta\lambda$ (nm) is the pulse spectral linewidth of each wavelength pulse within the code.

The effects of environmental temperature variation over the envelope of the autocorrelation signal (S_t), assuming each wavelength pulse has a Gaussian shape with a constant peak power P_p, are given by [10]

$$S_t = \sum_{k=0}^{\omega-1} P_p \exp\left\{-2.77\left[\frac{t - k\Delta t}{\tau - \Delta\tau}\right]^2\right\}, \tag{6}$$

where τ is the chip width (t_c).

Observe that S_t is the incoherent sum of w wavelength pulses present within the code at a decoder output after the code has been propagated in the link length d_{ij} under the effects of environmental temperature variation. On other hand, the height of the autocorrelation signal for 2D codes using w wavelengths pulses is w for an ideal case [3]. Furthermore, the power penalty caused by the environmental temperature variation ($P_{\Delta T}$) is defined as

$$P_{\Delta T} = 10\log_{10}\left(\frac{S_t}{\omega}\right). \tag{7}$$

IV. Power Control

A. Problem Statement

In OCDMA networks, power control appears to be a huge challenge, since the MAI introduces the near–far problem [15]. Furthermore, if the distances between the nodes are quite different like in real optical networks, the signal power received from various nodes will be significantly distinct. Thus, considering the star coupler as the reference, the performance of closer nodes is many orders of magnitude better than that of far ones. The solution based on the static power budget analysis establishes the transmitted power necessary to reach the photodiode sensibility [3]. The design based on a static power budget results in transmitted power higher or lower than the necessary transmitted power; then the increase of the near–far problem occurs [15]. To solve this problem, it is adequate to apply dynamic power control that defines the transmitted power according to the number of active transmitter nodes [17]. In this way, an efficient power control is needed to overcome this problem and enhance the performance and throughput of the network; this could be achieved through SNIR optimization [6,15,17]. In this context, the power control could be utilized to mitigate the effects of dynamic environmental temperature variation.

In this work, without loss of generality, the effects of temperature were isolated from the other effects of the transmissions through the optical fiber. Thus, we assumed laser sources with very short coherent length in order to isolate the effects of temperature from relative-intensity noise (RIN) and the beat-noise (BN) noise effects [3,10,18]. The RIN quantifies the amount of intensity fluctuation and exists for all sources; however, coherent light sources (i.e., lasers) generate negligible RIN because of their high damping ratio. Moreover, the BN directly depends on the coherent length of the laser sources used in the systems [18]. In addition, it was considered that the fiber link has been fully compensated for dispersion. In this context, in our model it was considered that the performance loss was due to temperature variations and the main limitation of OCDMA systems, i.e., the MAI. Herein, to avoid unreal simplification the receiver noise has been considered in our analysis.

In order to achieve a specific quality of service (QoS), which is associated with a maximum bit error rate (BER) tolerated by the ith optical node, the carrier-to-interference plus noise ratio (CINR) at the required decoder input can be defined as [15]

$$\Gamma_i = \frac{p_i G_{ii} G_{\text{amp}}}{G_{\text{amp}} \sum_{j=1, j\neq i}^{K} p_j G_{ij} + 2\sigma^2} \geq \Gamma^*, \tag{8}$$

where p_i is the ith node transmitted power, σ^2 is the power of receiving noise, and the value 2 takes into account two polarization modes presented in a single-mode fiber [15]. Γ^* is the established CINR target value, and the elements G_{ij}, that represent the connections of transmitter–receiver pairs, which are in linear units considering the power penalty caused by the environmental temperature variation, are given by

$$G_{ij} = a_{\text{star}} \exp(-\propto_f d_{ij}) L_C G_{\text{amp}} P_{\Delta T,i}, \tag{9}$$

where L_c is the summation of encoder and decoder losses.

Note that the usual receiver noise power σ^2 in Eq. (8) includes thermal noise, shot noise, and optical preamplifier noise. However, the ASE in the optical preamplifier will be the main limiting factor (in addition to the MAI), compared to thermal and shot noise at the receiver [15]. In this work, the receiver noise power is represented as [6]

$$\sigma^2 = 2n_{\mathrm{SP}}hf(G_{\mathrm{amp}} - 1)B_0, \tag{10}$$

where n_{SP} is the spontaneous emission factor, typically around 2–5, h is Planck's constant, f is the carrier frequency, G_{amp} is the amplifier gain, and B_o is the optical bandwidth. Ideally, to reduce the ASE noise power, the optical bandwidth can be set to a minimum of $B_o = 2R$, where R is the bit rate. In the case of 2D OCDMA networks, the SINR is obtained considering the N_T mean cross-correlation value, ρ_{2D}:

$$\gamma_i = \frac{N_T^2}{\rho_{2D}^2} \cdot \Gamma_i. \tag{11}$$

Defining the K-dimensional column vector of the transmitted optical power $\mathbf{p} = [p_1, p_2, \ldots, p_K]^T$, the optical power control problem consists of finding the optical power vector $\mathbf{p}$ that minimizes the cost function $J(\mathbf{p})$ and can be formulated as [15]

$$\min_{\mathbf{p}\in\mathbb{R}_+^K} J(\mathbf{p}) = \min_{\mathbf{p}\in\mathbb{R}_+^K} \mathbf{1}^T\mathbf{p} = \min_{p_i\in\mathbb{R}_+} \sum_{i=1}^{K} p_i, \tag{12}$$

subject to

$$\Gamma_i \geq \Gamma^*, \qquad \mathrm{P}_{\min} \leq p_i \leq \mathrm{P}_{\max}, \tag{13}$$

where $\mathbf{1}^T = [1, \ldots, 1]$ and Γ^* is the minimum CINR to achieve a desired QoS. Using matrix notations, Eq. (8) can be written as $[\mathbf{I} - \Gamma^*\mathbf{H}]\mathbf{p} \geq \mathbf{u}$, where $\mathbf{I}$ is the identity matrix, and $\mathbf{H}$ is the normalized interference matrix, whose elements are evaluated by $H_{ij} = G_{ij}/G_{ii}$ for $i \neq j$ and zero for another case; thus $u_i = \Gamma^*\sigma^2/G_{ii}$, where there is a scaled version of the noise power. Substituting inequality by equality, the optimized power-vector solution through the matrix inversion $\mathbf{p}^* = [\mathbf{I} - \Gamma^*\mathbf{H}]^{-1}\mathbf{u}$ could be obtained. This optical power vector represents the case of power equilibrium at the receiver node, and is then the optimal power required achieving the target CINR. The centralized power control obtained by matrix inversion is computationally intensive and corresponds to the existence of a central node [17]. The central node stores information about all physical network architecture, such as the fiber length between nodes and regular updates about transmission establishment and the dynamics of traffic. These characteristics are the drawbacks of centralized control [15]. On other hand, the power control based on PSO consists of the development of a heuristic procedure for the vector $\mathbf{p}$ evolution in order to reach their optimum value based on γ_i, γ^*, and p_i [19].

B. Particle Swarm Optimization

In the PSO process, each particle keeps track of its coordinates in the space of interest, which are associated with the best solution (fitness) it has achieved so far. Another best value tracked by the global version of the particle swarm optimizer is the overall best value and its location, obtained so far by any particle in the population. At each time iteration step, the PSO concept consists of velocity changes of each particle toward local and global locations. Acceleration is weighted by a random term, with separate random numbers being generated for acceleration toward local and global locations. Let b_p and v_p denote the particle coordinates (position) and its corresponding flight speed (velocity) in a search space, respectively. In this strategy, each power-vector candidate $\mathbf{b}_p[t]$, with dimension $K \times 1$, is used for the velocity-vector calculation of the next iteration [20]:

$$\begin{aligned}\mathbf{v}_p[t+1] = \omega[t] \cdot \mathbf{v}_p[t] + C_1 \cdot \mathbf{U}_{p1}[t](\mathbf{b}_p^{\mathrm{best}}[t] - \mathbf{b}_p[t]) \\ + C_2 \cdot \mathbf{U}_{p2}[t](\mathbf{b}_g^{\mathrm{best}}[t] - \mathbf{b}_p[t]),\end{aligned} \tag{14}$$

where $\omega[t]$ is the inertia weight of the previous velocity in the present speed calculation; the velocity-vector has K dimension $\mathbf{v}_p[t] = [\mathrm{v}_{p1}^t \mathrm{v}_{p2}^t \ldots \mathrm{v}_{p\mathrm{K}}^t]^T$; the diagonal matrices $\mathbf{U}_{p1}[t]$ and $\mathbf{U}_{p2}[t]$ with dimension K have their elements as random variables with uniform distribution $\sim U \in [0, 1]$, generated for the pth particle at iteration $t = 1, 2, \ldots, \mathcal{G}$; $\mathbf{b}_g^{\mathrm{best}}[t]$ and $\mathbf{b}_p^{\mathrm{best}}[t]$ are the best global vector-position and the best local vector-position found until the t_{th} iteration, respectively; and C_1 and C_2 are acceleration coefficients regarding the best particles and the best global positions' influences in the velocity updating, respectively. The p_{th} particle's position at the tth iteration is defined by the power candidate-vector $\mathbf{b}_p[t] = [\mathrm{b}_{p1}^t \mathrm{b}_{p2}^t \ldots \mathrm{b}_{p\mathrm{K}}^t]^T$. The position of each particle is updated using the new velocity vector for that particle,

$$\mathbf{b}_p[t+1] = \mathbf{b}_p[t] + \mathbf{v}_p[t+1], \qquad p = 1, \ldots, \mathcal{P}, \tag{15}$$

where $\mathcal{P}$ is the population size. In order to reduce the likelihood that the particle might leave the search universe, a maximum velocity factor $V_{\max}$ factor is added to the PSO model, which will be responsible for limiting the velocity to the range $[\pm V_{\max}]$.

The following maximization cost function could be employed as an alternative to OCDMA resource allocation optimization [19]:

$$\begin{aligned}J_1(\mathbf{p}) = \max \ & \frac{1}{K} \sum_{k=1}^{K} \mathcal{F}_k^{\mathrm{th}}\left(1 - \frac{p_k}{P_{\max}}\right) \\ & \gamma_k \geq \gamma_k^*, \quad 0 < p_k^l \leq P_{\max}, \quad R^l = R_{\min}^l \\ & \forall\, k \in K_l, \qquad \text{and } \forall\, l = 1, 2, \ldots, L,\end{aligned} \tag{16}$$

where L is the number of different groups of information rates allowed in the system, and K_l is the number of users in the lth rate group with minimum rate given by $R_{\min}^l$. The threshold function in Eq. (16) is simply defined as

$$\mathcal{F}_k^{\mathrm{th}} = \begin{cases} 1, & \gamma_i \geq \gamma^* \\ 0, & \text{otherwise} \end{cases}, \tag{17}$$

where the SNIR for the kth user, γ_i, is given by Eq. (11). The term $1 - \frac{p_k}{P_{\max}}$ gives credit to those solutions with minimum power and punishes others using high power levels [20].

C. Ant Colony Optimization

In the ACO process, the ants' behavior when looking for food has been applied for optimization purposes. In this context, each ant walks through the points of the input set, and deposits pheromones on its edges. The next point selection is done probabilistically, considering the amount of pheromones on each edge, jointly with the heuristic information. Given a set of points next to an ant, the probability of each of these points being chosen forms a probability mass function (PMF). The main idea of ACO is the change of this PMF to a probability density function (PDF); this way, an ant samples a continuous PDF instead of choosing a point next to it. This is because the continuous domain has infinite points to be chosen. The PDF used in this work is the Gaussian PDF given its soft capacity of generating random numbers, and due to the fact that it has only one maximum point located at the mean of the process. However, this last feature is not useful when the search space has more than one feasible region. To overcome this problem, the ACO uses a weighted sum of Gaussians with different means to sample each dimension of the problem. The essential steps in the ACO algorithm implementation as well as the input parameter optimization procedure, including the "file size," the "pheromone evaporation coefficient," the "population size," the "diversity parameter," and the "volatility coefficient," have been discussed in previous works [21]. The mathematical formalism for the ACO-based power control algorithm applicable to OCDMA was previously presented in [22] and will not be presented here since it is not the focus of this work.

V. Results

The main parameters utilized in the simulations are illustrated in Table I. Typical parameters related to devices, components, and equipment were assumed for 2D codes with code weight of 4 and 8, and code length of 200. Thus, the code is characterized by $(8 \times 200, w, 1, 0)$ for the transmission rate of 2.5 Gbps. The AWG encoder/decoder has approximately uniform loss of 6 dB independently of the number of wavelengths (N_λ) [15].

TABLE I
System Parameters

Variable	Value
α_f–Fiber loss coefficient	0.2 (dB/km)
d_{ij}–Link length	[4: 50] km
h–Planck constant	$6,63 \times 10^{-34}$ (J/Hz)
f–Light frequency	193,1 (THz)
B_o–Optical bandwidth	30 (GHz)
n_{sp}–Spontaneous emission factor	2
δ–Excess loss ratio	0.2 (dB)
G_{amp}–EDFA gain	20 (dB)
2D OCDM codes	$(8 \times 200, w, 1, 0)$
w–Code weight	4 and 8
T_C–Chip period	2 (ps)
D_{temp}–Thermal coefficient	0.0025 (ps/nm·km/°C)
ΔT–Change in temperature	[0: 20] (°C)
$\Delta\Lambda$–Spectral spacing	0.4 and 0.8 (nm)
$\Delta\lambda$–Pulse spectral linewidth	1.4 (nm)
γ^*–Target SNIR	20 dB
K–Number of nodes	4, 8, and 12

Initially, we presented in Fig. 2 the power penalty caused by the environmental temperature variation. The spectral spacing of 0.4 and 0.8 nm, and distance of 25 and 50 km, are considered for code weights of 8 [Fig. 2(a)] and 4 [Fig. 2(b)].

From Figs. 2(a) and 2(b), one could observe the increase of the power penalty with the increase of the temperature variation. The power penalty was more accentuated with the increase of the code weight and the increase of the distance. Furthermore, the power penalty increases with the increase of the spectral spacing. The increase of the code weight and spectral spacing will result in the temporal skewing increasing [12]. This effect occurs because the increase of the code weight and spectral spacing will increase the delay between the optical chip pulses resulting in a smaller autocorrelation in the receiver. Besides, the power penalty is directly related with temporal skewing. The results illustrated in Fig. 2 are in accordance with the previous results of autocorrelation described in [10,13].

The remainder of this section is composed of two subsections. First, a comparison between the PSO-based and ACO-based power control algorithms is conducted with the objective of illustrating the particularities of both heuristics in solving the power control problem with temperature variation. After that, the PSO power control algorithm is deployed and the main features to dynamically mitigate

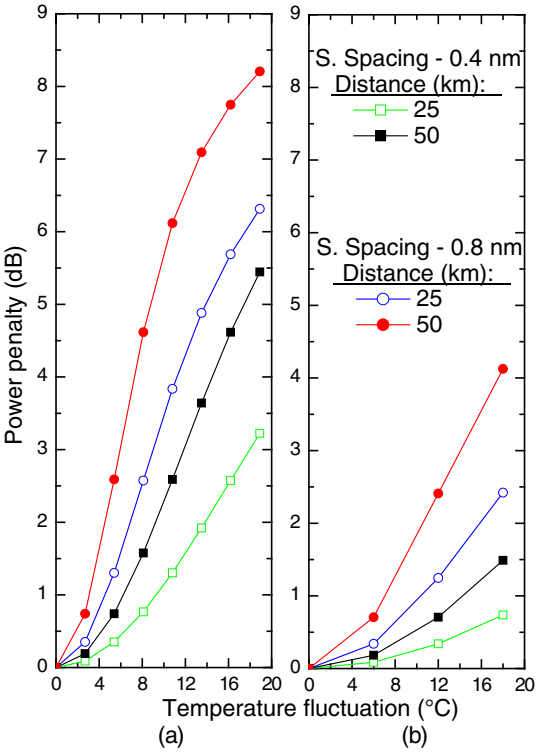

Fig. 2. Power penalty for temperature fluctuation considering spectral spacing of 0.4 and 0.8 nm and distance of 25 and 50 km for code weight of (a) 8 and (b) 4.

the effects of temperature variation are put into perspective.

A. PSO-Based and ACO-Based Power Control Performance

The main objective in this analysis is to put into perspective the PSO and ACO power control heuristic algorithms applied to dynamically mitigate the effects of temperature variation in OCDMA networks. The PSO and ACO power control algorithms present different computational complexity; as a consequence, the number of operations of sum and multiplication, as well as the number of iterations necessary to reach convergence results, are different [22,23]. In order to obtain a fair comparison between the PSO and ACO power control heuristic algorithms, the same computational effort, here represented by the run time, was warranted for both power control heuristic algorithms. In terms of the simulation setup, the run time settled is approximately 28, 81, and 192 s for the number of 4, 8, and 12 network nodes, respectively [22].

In Tables II and III we illustrate the PSO and ACO parameters utilized in our simulations, respectively. These parameters' optimizations were extensively discussed in [19,22] and are not the focus of this work.

Figure 3 depicts the transmitted power evolution of an OCDMA network with four nodes considering the effects of temperature variation for the PSO-based and ACO-based power control algorithms. The nodes are equally distributed over an area with a radius of 25 km; hence, the range of the total link length is 50 km for all four nodes. For instance, in each link a different temperature variation of 0, 10, 15, and 20 °C has been considered. A code weight of 4 and spectral spacing of 0.4 nm were considered in Figs. 3(a) and 3(b) for PSO and ACO power control algorithms, respectively. In addition, a code weight of 4 and spectral spacing of 0.8 nm were considered in Figs. 3(c) and 3(d) for PSO and ACO power control algorithms, respectively. To evaluate the convergence of the power control algorithms, the matrix inversion results are plotted with horizontal dotted lines.

TABLE II
PSO PARAMETERS

Variable	Value
$\mathcal{P}$–Number of particles	$\mathcal{P} = K + 2$
C_1–Particle acceleration	1.8
C_2–Global acceleration	2
$p_{\max}$–Maximum power	20 dBm
$p_{\min}$–Minimum power	$p_{\max} \times 10^{-12}$
ω–Inertial weight	$\omega[t] = (\omega_i - \omega_f)(\frac{\varphi - t}{\varphi})^m + \omega_f$
m–Nonlinear index	[0.6; 1.4]
φ–Number of iterations	1000
ω_i–Initial weight inertia	1
ω_f–Final weight inertia	0.4
$V_{\max}$–Maximum velocity	$V_{\max} = 0.2(p_{\max} - p_{\min})$
$V_{\min}$–Minimum velocity	$V_{\max} = -V_{\min}$

TABLE III
ACO PARAMETERS

Variable	Value
F_S–File size	7
ξ–Pheromone evaporation coefficient	1.3
m–Population	K
q–Diversity parameter	0.1

From Fig. 3, we could observe the convergence of the values of transmitted power from the PSO and ACO power control algorithms to the value obtained with matrix inversion. The effects of temperature variation in each node have been illustrated by the variation of the transmitted power. If no temperature variation is considered, all nodes will transmit the same power limited by the interference of other users (MAI). When Figs. 3(a) and 3(b) are compared with Figs. 3(c) and 3(d), we observe the influence of the code spectral spacing on the transmitted power to mitigate the environmental effects. The increase of the spectral spacing will result in the increase of power penalty caused by temporal skewing increasing. Observe that the PSO power control was able to achieve convergence after approximately

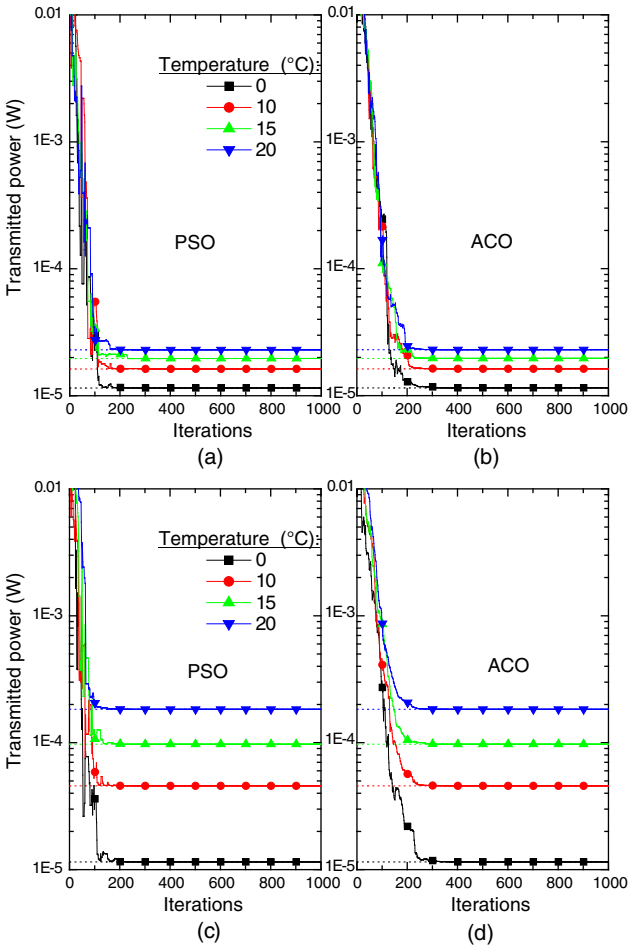

Fig. 3. Transmitted power for number of iterations considering a code weight of 4 and spectral spacing of 0.4 nm in (a) and (b), and 0.8 nm in (c) and (d).

the mean of 168 iterations in contrast to approximately the mean of 210 iterations necessary for the ACO power control convergence. The faster convergence of the PSO power control is obtained at the expense of the nonmonotonic oscillated convergence behavior, in contrast to the smoother, more monotonic convergence of the ACO-based power control OCDMA network algorithm.

Figure 4 shows the transmitted power evolution for a more complex network scenario constituted by eight nodes, considering the effects of temperature variation for the PSO-based and ACO-based power control algorithms. The nodes are distributed over an area with a radius of 3, 6, 9, 12, 15, 18, 21, and 24 km; hence, the range of the total link length is 6, 12, 18, 24, 30, 36, 42, and 48 km. For instance, in each link a temperature variation of 20 °C has been considered. A code weight of 4 and spectral spacing of 0.4 nm were considered in Figs. 4(a) and 4(b) for PSO and ACO power control algorithms, respectively. In addition, a code weight of 4 and spectral spacing of 0.8 nm were considered in Figs. 3(c) and 3(d) for PSO and ACO power control algorithms, respectively. Again, to evaluate the convergence of the power control algorithms, the matrix inversion results are plotted and represented by horizontal dotted lines.

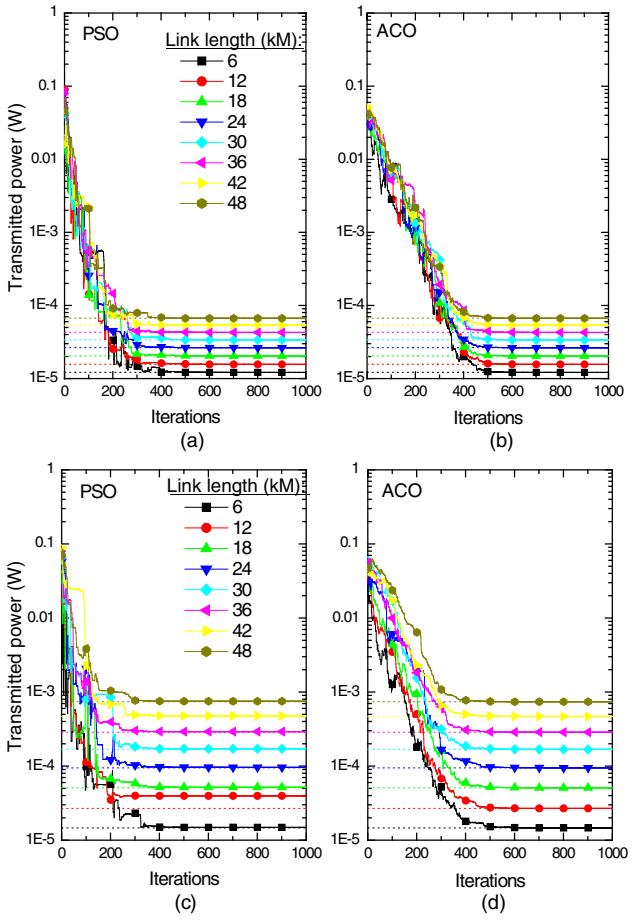

Fig. 4. Transmitted power for number of iterations considering a code weight of 4 and spectral spacing of 0.4 nm in (a) and (b), and 0.8 nm in (c) and (d).

One can see from Fig. 4 that the transmitted power values obtained by the PSO-based and ACO-based power control algorithms converge to the values obtained with matrix inversion, which could be observed for different link lengths. If no distance variation is considered, all nodes will transmit the same power limited by the interference of other users. As expected, the far node will transmit with the highest power. Therefore, we observe the effects of MAI related with the number of nodes, the near–far effect related with different link lengths, and the effects of temperature variation. The influence of the code spectral spacing is similar to that discussed in Fig. 3. Notice that the PSO power control was able to achieve convergence after approximately the mean of 310 iterations in contrast to the approximately 400 iterations necessary for the ACO power control convergence. Furthermore, the same nonmonotonic oscillated convergence behavior of PSO power control observed in Fig. 3 is also present in Fig. 4. This behavior is related with the capability of the algorithm to execute a broad global search aiming to escape from local optima solutions.

Hence, from Figs. 3 and 4 the average number of iterations necessary for the PSO-based and ACO-based power control algorithms to achieve convergence has been quantified. However, the quality of the solutions has not been clearly evaluated yet. In order to evaluate the quality of solution achieved by the PSO- and ACO-based power control algorithms, the normalized mean squared error (NMSE) must be introduced. The NMSE is a measurement of how close to the optimum solution the found solution is (after t iterations). For the power allocation problem, the NMSE definition is given by [22]

$$\mathrm{NMSE}[t] = \mathbb{E}\left[\frac{\|\mathbf{p}[t] - \mathbf{p}^*\|^2}{\|\mathbf{p}^*\|^2}\right], \tag{18}$$

where $\|\cdot\|^2$ denotes the squared Euclidean distance, $\mathbf{p}[t]$ represents the transmitted power after tth iterations, $\mathbf{p}^*$ is the optimum transmitted power obtained by matrix inversion, and $\mathbb{E}[\cdot]$ is the expectation operator.

Figure 5 shows the decrease of the NMSE with the evolution of the number of iterations. One can observe that the increasing number of network nodes affects the performance of both PSO-based and ACO-based power control algorithms. This occurs because the problem of optimum power allocation is not straightforward, since the cost function and constraint functions are not convex. Thus, the nonconvexity of the problem increases the number of local optima. In addition, for comparison purposes, note that the behavior of the NMSE is very close for both power control algorithms. In fact, the NMSE for the PSO-based power control algorithm is a little lower than the NMSE for the ACO power control algorithm until a certain number of iterations, i.e., for the analyzed system scenarios, these numbers are approximately 485, 576, and 678 iterations for 4, 8, and 12 network nodes, respectively. After this point, there is an inversion in this tendency and the NMSE for the ACO-based power control algorithm becomes lower than the NMSE for the PSO-based power control algorithm. This trend illustrates that both PSO and ACO power

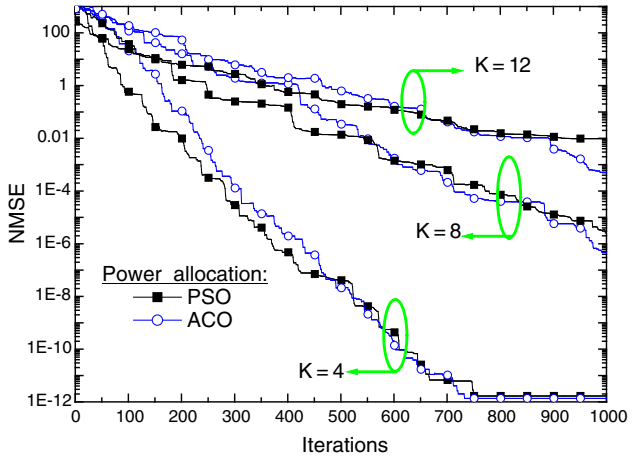

Fig. 5. NMSE for the number of iterations considering 4, 8, and 12 network nodes for power control algorithms based on PSO and ACO.

control algorithms in OCDMA networks present similar performance-complexity trade-off (same order), taking into account the same quality of solutions.

In summary, the PSO and ACO power control heuristic algorithms are effective to dynamically mitigate the effects of temperature variation. However, when the objective in achieving low computational effort must be considered (for implementability purposes), the PSO-based power control algorithm was able to achieve convergence a little earlier than the ACO-based power control algorithm for the same low computational complexity constraint.

The faster convergence of the PSO-based power control for the OCDMA network is obtained at the expense of the nonmonotonic oscillated convergence behavior, in contrast to the smoother, more monotonic convergence of the ACO power control algorithm.

B. PSO-Based Power Control in OCDMA Networks With Temperature Variation

In the remainder of this study, the PSO power control algorithm will be applied to dynamically mitigate the effects of temperature variation in a network with different link lengths and temperature variation. The optical network scenario considered is presented in Fig. 6, where a network with 12 nodes has been considered. Figures 6(a) and 6(b) depict the link length from the transmitting nodes to the star coupler and the link length from the receiving nodes to the star coupler, respectively. The nodes are uniformly distributed over an area with a radius between 2 and 25 km; hence, the range of the total link length is [4; 50] km. This topology, such as the number of nodes, code parameters, and node distances, is compatible with the previous OCDMA networks considering environmental temperature variation [10,13]. This network configuration can be adapted to standard patterns, such as 10GE-PON, or to an increasing number of the nodes [15]. Furthermore, Fig. 7 illustrates the temperature variation uniformly

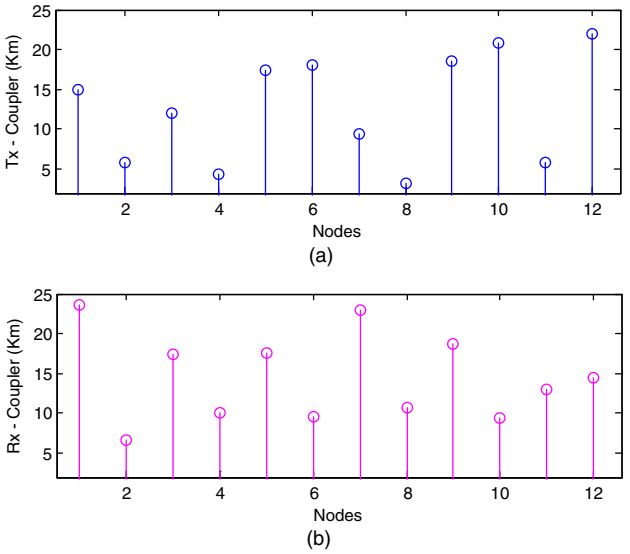

Fig. 6. Network node distances from (a) transmitter (ith node) to the star coupler and (b) receiver (ith node) to the star coupler.

distributed between 15 and 20 °C for the 12 links between the Tx-coupler and the Rx-coupler.

In order to evaluate the mitigation of the environmental temperature variation effects, the numerical results presented in Fig. 8 show the sum of the transmitted power evolution from all nodes with respect to the number of iterations, considering spectral spacing of 0.4 and 0.8 nm. Code weights of $w = 8$ and $w = 4$ were considered in Figs. 8(a) and 8(b), respectively. In order to evaluate the convergence of the PSO-based power control algorithm, the matrix inversion results are plotted with horizontal dotted lines.

From Figs. 8(a) and 8(b), we could observe the convergence of the values of transmitted power from the PSO-based power control algorithm to the value obtained with matrix inversion. The power control algorithm considered in this work could be calculated without the need for matrix inversion, which is computationally more intensive. The target SNIR established for all the nodes is equal to 20 dB, and if the perfect power balancing with no environmental temperature variation effects is assumed, it could be demonstrated that the maximum SNIR and the transmitted power will be defined by the number of optical nodes in the network. However, when the environmental

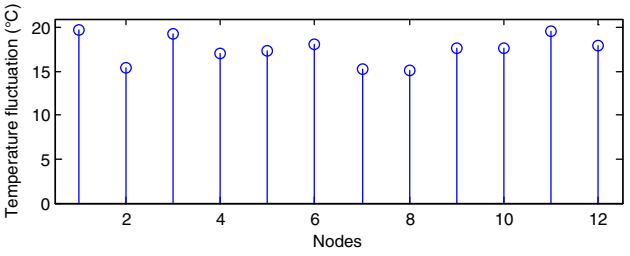

Fig. 7. Temperature deviation in each node of the optical OCDMA network.

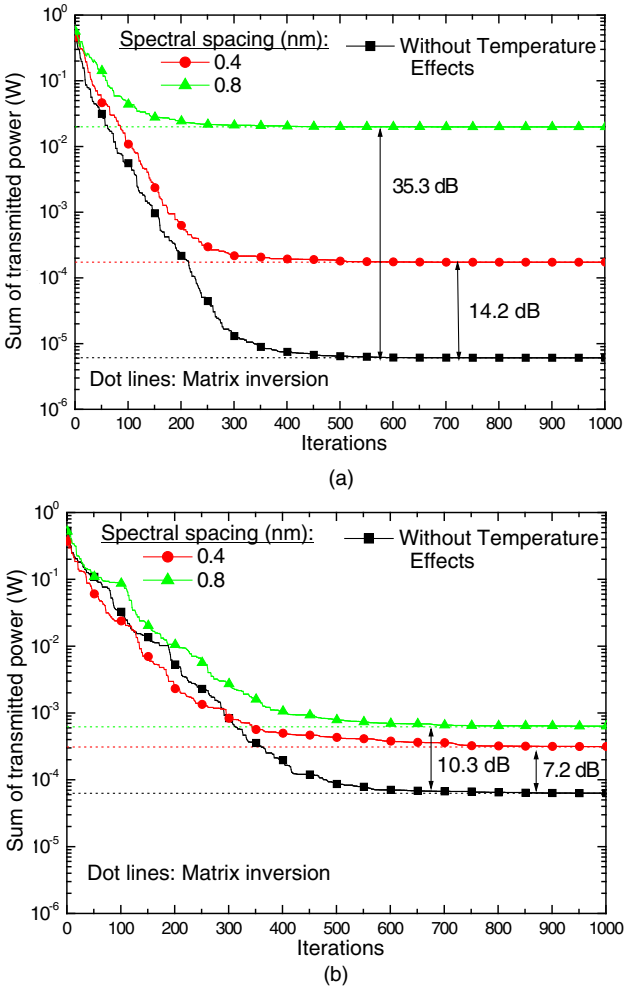

Fig. 8. Sum of transmitted power for number of iterations considering spectral spacing of 0.4 and 0.8 nm for code weight of (a) $w = 8$ and (b) $w = 4$.

temperature variation effects are considered, there is a power penalty. This penalty represents the received power reduction due to temporal skewing. Figure 8(a) shows the increment in the transmitted power to mitigate the environmental effects for code weight of 8. This increment is 35.3 and 14.2 dB for spectral spacing of 0.4 and 0.8 nm, respectively. On other hand, Fig. 8(b) shows the increment in the total transmitted power to mitigate the environmental effects to code weight of 4. This increment is 10.3 and 7.2 dB for spectral spacing of 0.4 and 0.8 nm, respectively. Thus, lower spectral spacings are more robust to the environmental temperature variation effects. This effect occurs because optical codes with lower spectral spacing present small deviations of optical pulses in the receiver under skewing effects [10].

When Figs. 8(a) and 8(b) are compared, we observe the influence of the code weight on the transmitted power to mitigate the environmental effects. As expected, without the influence of the environmental effects, the transmitted power is lower for higher code weight compared with lower code weight. Therefore, the transmitted power for code weight of 8 [Fig. 8(a)] is lower than for code weight of 4 [Fig. 8(b)]. The code variance is inversely proportional with code weight; thus for higher code weight there is lower variance [3]. According to lower variance, the transmitted power to achieve the target SNIR is lower [15]. However, when environmental effects are considered, the transmitted power is lower for lower code weights, because for higher code weight there is probability to increase the delay between optical code chips.

Figure 9 shows the transmitted power for each node considering the effects of temperature variation to spectral spacing of 0.4 and 0.8 nm. The transmitted power of each node for the case without temperature effects is also illustrated. Code weights of 8 and 4 were considered in Figs. 9(a) and 9(b), respectively.

From Figs. 9(a) and 9(b), we could observe the effects of temperature variation in each node. The same tendency of the effects of temperature variation observed in the previous results was confirmed here for the same code parameters; besides, it is possible to verify the interference of other users (MAI) together with temperature effects. For

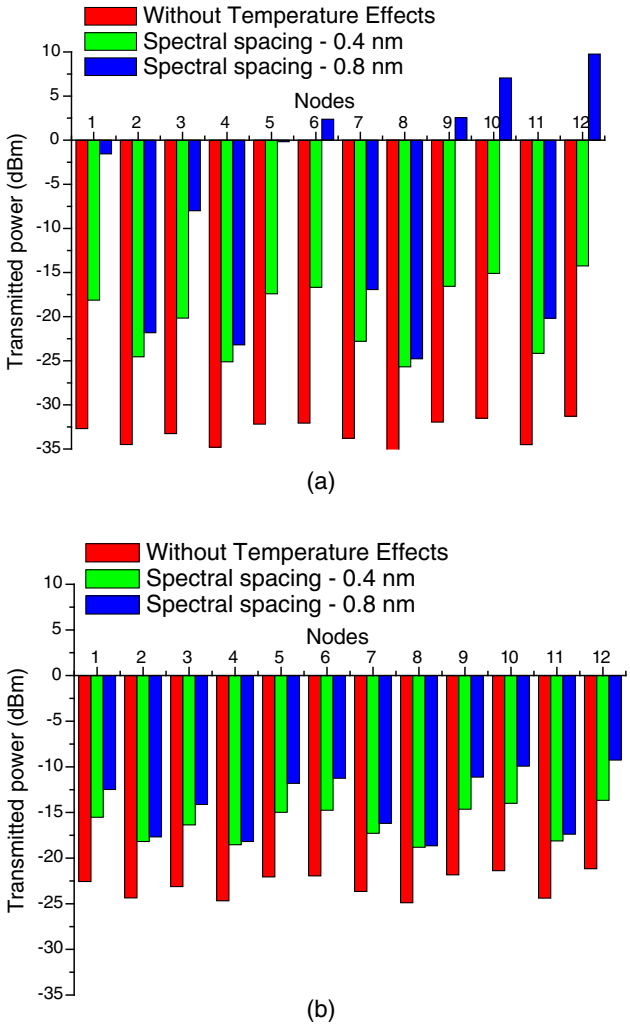

Fig. 9. Transmitted power for each node considering spectral spacing of 0.4 and 0.8 nm for code weight of (a) $w = 8$ and (b) $w = 4$.

example, for node 6 considering the code weight of 4 in Fig. 9(b), the transmitted power is approximately −21.8 dBm when no temperature variation is considered. On other hand, the transmitted power increases to −14.8 and −11.2 dBm when the temperature variation is considered for code spectral spacing of 0.4 and 0.8 nm, respectively. In this context, we observe the increase of MAI when the skewing caused by temperature variation increases. This effect results from the decrease of the autocorrelation height caused by temperature effects, and the distortion of the shape, as well as the width of the decoded autocorrelation signal caused by the interference of other nodes.

VI. Conclusions

In this work, a heuristic power control approach based on PSO is proposed to efficiently mitigate the environmental temperature variation effects in 2D (time/wavelength) OCDMA networks. The environmental temperature variation can generate time skewing in which a temporal spreading of multiwavelength pulses and relative delays occur among chips at different wavelengths. In this sense, even links with full compensation of the dispersion effect can experience incorrect decoding and then errors in bit detection.

The main idea is the utilization of the PSO-based power control algorithm to dynamically adjust the intensity of the transmitted optical power from the laser source with respect to the target SNIR.

Our numerical results have illustrated the effectiveness of the proposed PSO-based power control algorithm when compared with other heuristic power control algorithms based on ACO. The PSO-based power control algorithm was able to achieve convergence a little earlier than the ACO-based power control algorithm with satisfactory quality of solutions when the same computational run time was considered. The faster convergence of the PSO power control is obtained at the expense of the nonmonotonic oscillated convergence behavior, in contrast to the smoother, more monotonic convergence of the ACO-based power control algorithm.

The effects of the code parameters, namely the code weight and the spectral spacing, were evaluated for a numerical example considering a temperature variation between 15 and 20 °C for an OCDMA network with 12 network nodes. Herein, the lower power penalty was observed for a code weight of 4 confronted with code weight of 8. For a code weight of 4, an increment in the sum of transmitted power of 10.3 and 7.2 dB for spectral spacing of 0.4 and 0.8 nm, respectively, was observed. Thus, lower code weight and lower spectral spacing are more robust to the environmental temperature variation effects; thus lower power should be transmitted to achieve the target SNIR when compared with higher code weight and spectral spacing. In this context, the proposed PSO-based power control mechanism for the transmitted powers is quite effective in order to dynamically mitigate the effects of temperature variation with low cost and competitive computational complexity.

Acknowledgments.

This research was funded by the Araucaria Foundation (668/2014) and the National Council for Scientific and Technological Development (CNPq) (446995/2014-2).

References

[1] D. Kilper, K. Bergman, V. W. S. Chen, I. Monga, G. Porter, and K. Rauschenbach, “Optical networks come of age,” *Opt. Photonics News*, vol. 25, no. 9, pp. 50–57, Sept. 2014.

[2] I. Tomkos, S. Azodolmolky, J. Solé-Pareta, D. Careglio, and E. Palkopoulou, “A tutorial on the flexible optical networking paradigm: state-of-the-art, trends, and research challenges,” *Proc. IEEE*, vol. 102, no. 9, pp. 1317–1337, Sept. 2014.

[3] H. Yin and D. J. Richardson, *Optical Code Division Multiple Access Communication Networks: Theory and Applications.*, Berlin: Springer-Verlag and Tsinghua University, 2009.

[4] K. Fouli and M. Maier, “OCDMA and optical coding: principles, applications, and challenges,” *IEEE Comm. Magazine*, vol. 45, no. 8, pp. 27–34, Aug. 2007.

[5] E. Inaty, R. Raad, P. Fortier, and H. M. H. Shalaby, “A fair QoS-based resource allocation scheme for a time-slotted optical OV-CDMA packet network: a unified approach,” *J. Lightwave Technol.*, vol. 26, no. 21, pp. 1–10, Jan. 2009.

[6] F. R. Durand and T. Abrão, “Distributed SNIR optimization based on the Verhulst model in optical code path routed networks with physical constraints,” *J. Opt. Commun. Netw.*, vol. 3, no. 9, pp. 683–691, Sept. 2011.

[7] E. Mutafungwa, “Comparative analysis of the traffic performance of fiber-impairment limited WDM and hybrid OCDM/WDM networks,” *Photon. Netw. Commun.*, vol. 13, pp. 53–66, Jan. 2007.

[8] F. R. Durand, M. L. F. Abbade, F. R. Barbosa, and E. Moschim, “Design of multi-rate optical code paths considering polarisation mode dispersion limitations,” *IET Commun.*, vol. 4, no. 2, pp. 234–239, Jan. 2010.

[9] H. Lundqvist and G. Karlsson, “On error-correction coding for CDMA PON,” *J. Lightwave Technol.*, vol. 23, no. 8, pp. 2342–2351, Aug. 2005.

[10] T. B. Osadola, S. K. Idris, I. Glesk, and W. C. Kwong, “Effect of variations in environmental temperature on 2D-WH/TS OCDMA code performance,” *J. Opt. Commun. Netw.*, vol. 5, no. 1, pp. 68–73, Jan. 2013.

[11] G. Ghosh, M. Endo, and T. Iwasaki, “Temperature-dependent Sellmeier coefficients and chromatic dispersions for some optical fiber glasses,” *J. Lightwave Technol.*, vol. 12, no. 8, pp. 1338–1342, Aug. 1994.

[12] E. K. H. Ng, G. E. Weichenberg, and E. H. Sargent, “Dispersion in multi-wavelength optical code division multiple access systems: impact and remedies,” *IEEE Trans. Commun.*, vol. 50, no. 11, pp. 1811–1816, Nov. 2002.

[13] J. V. dos Reis, T. R. Raddo, A. L. Sanches, and B.-H. V. Borges, “Mitigation of environmental temperature variation effects using fuzzy systems and source-matched spreading codes for OCDMA networks,” in *Int. Conf. on Transparent Optical Networks (ICTON)*, Graz, Austria, July 6, 2014, pp. 1–6.

[14] M. Tang, C. Long, and X. Guan, “Nonconvex optimization for power control in wireless CDMA networks,” *Wireless Personal Commun.*, vol. 58, no. 4, pp. 851–865, 2011.

[15] N. Tarhuni, T. Korhonen, M. Elmusrati, and E. Mutafungwa, “Power control of optical CDMA star networks,” *Opt. Commun.*, vol. 259, pp. 655–664, Mar. 2006.

[16] Y.-K. Huang, V. Baby, I. Glesk, C.-S. Bres, C. M. Greiner, D. Iazikov, T. W. Mossberg, and P. R. Prucnal, "Novel multicode-processing platform for wavelength-hopping time-spreading optical CDMA: a path to device miniaturization and enhanced network functionality," *IEEE J. Sel. Top. Quantum Electron.*, vol. 13, no. 5, pp. 1471–1479, Sept./Oct. 2007.

[17] F. R. Durand, M. S. Filho, and T. Abrão, "The effects of power control on the optical CDMA random access protocol," *Opt. Switching Netw.*, vol. 9, no. 1, pp. 52–60, Jan. 2012.

[18] C.-S. Bres, Y.-K. Huang, D. Rand, I. Glesk, P. R. Prucnal, T. M. Bazan, C. Michie, D. Harle, and I. Andonovic, "On the experimental characterization of beat noise in 2-D time-spreading wavelength-hopping OCDMA systems," *IEEE Photonics Technol. Lett.*, vol. 18, no. 21, pp. 2314–2316, Nov. 2006.

[19] F. Durand and T. Abrão, "Energy-efficient power allocation for WDM/OCDM networks with particle swarm optimization," *J. Opt. Commun. Netw.*, vol. 5, no. 5, pp. 512–523, May 2013.

[20] H. Elkamchouchi, H. EIragal, and M. Makar, "Power control in CDMA system using particle swarm optimization," in *24th National Radio Science Conf.*, Cairo, Egypt, Mar. 13, 2007, pp. 1–8.

[21] K. Socha and M. Dorigo, "Ant colony optimization for continuous domains," *Eur. J. Oper. Res.*, vol. 185, no. 3, pp. 1155–1173, Mar. 2008.

[22] M. P. Marques, F. R. Durand, and T. Abrão, "WDM/OCDM energy-efficient networks based on heuristic ant colony optimization," *IEEE Syst. J.*, in press, doi:10.1109/JSYST.2014.2345665.

[23] L. Sampaio, T. Abrão, B. Angelico, M. Lima, M. Proença, and P. Jeszensky, "Hybrid heuristic-waterfilling game theory approach in MC-CDMA resource allocation," *Appl. Soft Comput.*, vol. 12, pp. 1902–1912, 2011.

Alysson José dos Santos received a B. S. in electrical engineering from the North Paraná University in 2006. He is currently pursuing a Masters Degree at the Electrical Engineering Department of UEL—State University of Londrina (Brazil).

Fábio R. Durand received an M.S. degree in electrical engineering from the São Carlos Engineering School of São Paulo State, Brazil, in 2002, and a Ph.D. in electrical engineering from the State University of Campinas (UNICAMP), São Paulo, Brazil, in 2007. He is now a Professor at the Technologic Federal University of Paraná (UTFPR) at Cornélio Procópio, Brazil. His research interests are in photonic technology, WDM/OCDM networks, the heuristic and optimization aspects of OCDMA networks, and PMD impairments.

Taufik Abrão (SM'12, SM-SBrT) received B.S., M.Sc., and Ph.D. degrees in electrical engineering from the Polytechnic School of the University of São Paulo, São Paulo, Brazil, in 1992, 1996, and 2001, respectively. Since March 1997, he has been with the Communications Group, Department of Electrical Engineering, Londrina State University, Londrina, Brazil, where he is currently an Associate Professor of Communications Engineering. In 2012, he was an Academic Visitor with the Communications, Signal Processing and Control Research Group, University of Southampton, Southampton, UK. From 2007 to 2008, he was a Post-doctoral Researcher with the Department of Signal Theory and Communications, Polytechnic University of Catalonia (TSC/UPC), Barcelona, Spain. He has participated in several projects funded by government agencies and industrial companies. He is involved in editorial board activities of six journals in the communication area, and he has served as a TCP member for several symposiums and conferences. He has served as an Editor for IEEE Communications Surveys & Tutorials since 2013 and the IET Journal of Engineering since 2014. He is a senior member of the IEEE and SBrT-Brazil. His current research interests include communications and signal processing, especially multi-user detection and estimation, MC-CDMA and MIMO systems, cooperative communication and relaying, resource allocation, as well as the heuristic and convex optimization aspects of 3G and 4G wireless systems. He has co-authored more than 200 research papers published in specialized/international journals and conferences.